Original Research Paper

Auricularia auricular polysaccharide-low molecular weight chitosan polyelectrolyte complex nanoparticles: Preparation and characterization

CrossMark

Wei Xiong [a], Qiantao Zhang [b], Fei Yin [c], Shihui Yu [a], Tiantian Ye [a], Weisan Pan [a], Xinggang Yang [a,*]

[a] School of Pharmacy, Shenyang Pharmaceutical University, 103 Wenhua Road, Shenyang 10016, China
[b] Shanxi Institute of International Trade&commerce, Tongyi Rd, Qindu, Xianyang, Shaanxi 712046, China
[c] Department of Pharmacy, Liaoning Cancer Hospital and Institute, 44 Xiaoheyan Road, Shenyang 110042, China

ARTICLE INFO

ABSTRACT

Novel polyelectrolyte complex nanoparticles (AAP/LCS NPs) were prepared in this study and these were produced by mixing negatively charged auricularia auricular polysaccharide (AAP) with positively charged low molecular weight chitosan (LCS) in an aqueous medium. The AAP was extracted and purified from auricularia auricular, and then characterized by micrOTOF-Q mass spectrometry, UV/Vis spectrophotometry, moisture analyzer and SEM. The yield, moisture, and total sugar content of the AAP were 4.5%, 6.2% and 90.12% (w/w), respectively. The AAP sample was water-soluble and exhibited white flocculence. The characteristics of AAP/LCS NPs, such as the particle size, zeta potential, morphology, FT-IR spectra, DSC were investigated. The results obtained revealed that the AAP/LCS NPs had a spherical shape with a diameter of 223 nm and a smooth surface, and the results of the FT-IR spectra and DSC investigations indicated that there was an electrostatic interaction between the two polyelectrolyte polymers. Bovine serum albumin (BSA, pI = 4.8) and bovine hemoglobin (BHb, pI = 6.8) were used as model drugs to investigate the loading and release features of the AAP/LCS NPs. The results obtained showed that the AAP/LCS NPs had a higher entrapment efficiency (92.6%) for BHb than for BSA (81.5%). The cumulative release of BSA and BHb from AAP/LCS NPs after 24 h in vitro was 95.4% and 91.9%, respectively. The in vitro release demonstrated that AAP/LCS NPs provided a sustained release matrix suitable for the delivery of protein drugs. These studies demonstrate that AAP/LCS NPs have a very promising potential as a delivery system for protein drugs.

* Corresponding author. Shenyang Pharmaceutical University, No.103, Wenhua Road, Shenyang 110016, China. Tel.: +86 24 23986313; fax: +86 24 23953241.
E-mail address: yangxg123@163.com (X. Yang).

1. Introduction

Currently, over 160 therapeutic protein drugs have been licensed, and even more protein drugs will be approved by regulatory agencies in the next few years [1]. The physico-chemical and biological properties of protein drugs are unlike those of conventional ones, particularly with regard to their molecular weight, solubility, physico-chemical stability, biological half-life, conformational stability, oral bioavailability, dose requirements, and administration [2]. Moreover, oral protein drugs usually exhibit a low level of bioavailability. The major challenges to be overcome involve poor protein absorption and internalization through the gastrointestinal epithelium, as well as the rapid hydrolysis and degradation by gastrointestinal fluids [3,4]. Hence, the design and manufacturing of delivery systems for protein is attracting much attention.

In order to overcome the above obstacles and increase the gastrointestinal uptake, some nanoparticles made from natural biodegradable polymers have been exploited and applied to protein drugs [5,6]. However, biodegradable polymer nanoparticles made from polyglycolic acid and polylactide and their copolymers are usually obtained by using organic solvents, high temperatures and sheer forces and are easily inactivated by physical and chemical denaturation. Furthermore, after the formulation has been administered, changes in the microenvironment can lead to polymer degradation which can dramatically affect the tertiary structure of the protein [7,8].

Entrapping protein drugs within polysaccharide nanoparticles is an effective way of protecting them from degradation in the gastrointestinal fluids, delivering protein drugs to the target sites for release and increasing their permeation across the gastrointestinal epithelium [9–11]. Natural polysaccharides have many promising properties, including excellent biodegradability, high biocompatibility, low toxicity, good safety, abundant availability, and their cost of production is low [12]. Moreover, most polysaccharides have hydrophilic groups, such as hydroxyl, carboxyl, and amino groups, which may form non-covalent bonds with biological tissues like the intestinal mucosa to facilitate the absorption of protein drugs [13,14].

Consequently, many references [5,15] have described how polyelectrolyte complex (PEC) nanoparticles are formed spontaneously by mixing oppositely charged polyelectrolytes in aqueous media without any chemical covalent cross-linker [16,17], and such PEC nanoparticles have bright application prospects for protein drugs. The major interactions between the two polyelectrolyte polymers are electrostatic, formation of hydrogen and hydrophobic bonds, as well as dipole–dipole association [18].

Auricularia auricular polysaccharide (AAP) is abundant in auricularia auricular, and is a significant bioactive substance, with broad physiological activity and which is attracting much attention because of its potential medical applications [19]. However, AAP as a novel natural polysaccharide has not been studied in any detail with regard to its use as a drug carrier. Hence, in this study, we used AAP as a negatively charged polyelectrolyte to form PEC with Chitosan (a cationic polyelectrolyte in acidic medium).

Based on the reasons mentioned above, the goal of this paper is to manufacture AAP/LCS NPs, composed of positively charged low molecular weight chitosan (LCS) and negatively charged AAP. Two model protein drugs with different pI values, BSA (pI = 4.8) and BHb (pI = 6.8), were used to investigate the protein loading capacity and release of AAP/LCS NPs. The physico-chemical characteristics of the prepared nanoparticles were characterized by investigation of Fourier transform infrared spectra (FT-IR), particle size, zeta potential, differential scanning calorimetry (DSC) and transmission electron microscopy (TEM). The results obtained indicated that novel AAP/LCS NPs had a very promising potential as a delivery system for protein drugs.

2. Materials and methods

2.1. Materials

Bovine serum albumin (BSA) and bovine hemoglobin (BHb) were purchased from Sigma–Aldrich (St. Louis, MO, USA). Coomassie brilliant blue G-250 was obtained from Regent Chemicals Co., Ltd (Tianjin, China). Auricularia auricular was bought from a Carrefour supermarket (Shenyang, China), and it had been grown in Liaoning Province, China. Low molecular weight chitosan was purchased from Golden-Shell Pharmaceutical Co., Ltd (Zhejiang, China), and the degree of deacetylation was 90%. All other reagents and chemicals were of analytical grade.

2.2. Extraction and purification of AAP

The AAP was extracted and purified by a modified water extraction and alcohol precipitation method [20]. For this, the auricularia auricular was defatted by reflux, dried and the resulting powder was weighed and extracted, then subjected to precipitation and washing with ethanol, to obtain crude grey polysaccharide by vacuum-drying. A 2% crude polysaccharide solution was prepared by removing protein by the Sevag method (chloroform: n-butanol = 4:1). The pH was adjusted to 8.0 with ammonia, and the color was removed with hydrogen peroxide. Then, the decolorized polysaccharide solution was dialyzed against distilled water and purified AAP was obtained by concentrating and freeze-drying the dialysate.

2.3. Characterization of AAP

2.3.1. Polysaccharide content

The AAP content was measured by phenol-sulfuric acid method using D-glucose as a standard [21]. The percentage of AAP extraction yield (%) was calculated with the formula as follow:

$$Yield\ (\%) = \frac{W_2}{W_1} \times 100 \tag{1}$$

Where W_2 is the polysaccharides content of extraction, and W_1 represents the dried sample weight.

The protein of the polysaccharide was detected by UV-4802 Double Beam UV/Vis Spectrophotometer (Unico, Shanghai, China). The moisture content of the AAP was obtained by a moisture analyzer (Shuangquan, Shanghai, China).

2.3.2. Molecular weight (Mw)

The molecular weight of the AAP was determined by time-of-flight mass spectrometry (Bruker micrOTOF-Q, Ettlingen, Germany). The LC-Q-TOF/MS instrument parameters were as follows: electrospray ionization (ESI) detection mode, capillary voltage 4.5 kV, capillary exit voltage –500 V; collision cell RF voltage 800 Vpp; capillary temperature 180 °C; N_2 was used as the fog and auxiliary gas and the flow rate was 4 mL/min. Argon was used as the collision gas for CID experiments, and the collision energy was 20 eV. The analytical data were collected in full scan mode from 50 m/z to 900 m/z.

2.3.3. SEM

The morphology and structural characteristics of the AAP were examined by SEM (SSX-550, Shimadzu, Japan). Each sample was thinly sprinkled onto a metal stub and vacuum-coated with a thin layer of gold in an argon atmosphere. The coated samples were examined at an acceleration voltage of 15 kV.

2.4. Preparation of AAP/LCS NPs

The AAP/LCS NPs were prepared by a modified coacervation method [22]. Preliminary experiments indicated that the concentration of AAP and LCS would affect the particle size and appearance. As a result, the concentrations of AAP and LCS were selected as two independent variables. AAP was dissolved in 5 mL deionized water, similarly, while LCS was dissolved in 5 mL acetic acid solution. The LCS solution was added slowly to the AAP solution with magnetic stirring for half an hour at room temperature. BSA or BHb AAP/LCS NPs were produced by the method described above (Method A), except that different amounts of BSA or BHb were dissolved in the LCS solution (1.0 mg/ml) before adding the AAP solution. In an adjusted method (Method B), nanoparticles were prepared by adding protein to the AAP solution (2.5 mg/ml). In Method C the protein were added to an AAP/LCS NPs suspension with magnetic stirring for half an hour.

2.5. Characterization of AAP/LCS NPs

2.5.1. pH measurement

The pH value of samples was measured at 20 ± 0.1 °C in a Sartorius PB-10 standard pH meter with an error of 0.01 pH units. The pH-meter was calibrated with two buffer solutions before use.

2.5.2. FT-IR spectroscopy

Fourier transform infrared spectra (Bruker IFS55FTIR, Ettlingen, Germany) was recorded in the KBr method to identify the functional groups that might be involved in the formation of the nanoparticles, to investigate the interaction between the $-NH_3^+$ of LCS and the $-COO^-$ of AAP.

2.5.3. DSC

The thermal properties of the samples were examined by DSC (DSC-60, Shimadzu, Japan). The samples were scanned at a heating speed of 5 °C/min over a temperature range of 20–300 °C with a nitrogen purge of 40 mL/min in aluminum pans sealed hermetically, using aluminum oxide as a reference. The melting point and crystallization point corresponded to the maximum and minimum, respectively, of the DSC curves.

2.5.4. Particle size and zeta potential and morphology

The mean particle size, polydispersity index, and zeta potential were determined using a Zeta-sizer Nano instrument (Malvern Instruments, UK) at room temperature. Each measurement was performed in triplicate. TEM (JEM-1200EX JEOL, Tokyo, Japan) was used to investigate the morphology of AAP/LCS NPs. Briefly, the samples were applied to carbon-coated copper grids, blotted, washed, negatively stained with 2% (w/v) phosphotungstic acid, air dried, and then observed directly by TEM.

2.6. Determination of entrapment efficiency (EE) and loading capacity (LC)

The protein-loaded AAP/LCS NPs were separated from the suspension by centrifugation at 20, 000 rpm for 30 min, 5 °C. The supernatant of the non-loaded protein was stained by the Coomassie Blue Method. The EE and LC of the nanoparticles were calculated as follows:

$$EE\,(\%) = \frac{W_T - W_F}{W_T} \times 100 \tag{2}$$

$$LC\,(\%) = \frac{W_T - W_F}{W_N} \times 100 \tag{3}$$

Where the W_T was the total weight of protein, the W_F was the weight of free protein and W_N was the weight of protein-loaded AAP/LCS NPs.

2.7. Evaluation of nanoparticles stability

The stability of the nanoparticles was investigated in a buffer solution (pH 1.2 and 7.4, respectively) at room temperature, which simulated the pH conditions in the GI tract. Fresh suspensions of nanoparticles were diluted with buffer solution and then the particle size of the drug-loaded nanoparticles was measured for several hours at room temperature.

2.8. In vitro release

Protein-loaded AAP/LCS NPs release studies were carried out by the dialysis technique. For this, 2 mL samples of suspension were placed in a pre-soaked dialysis bag (8000–12,000 molecular weight cut-off) and put in conical flask containing 50 mL buffer solution (pH 1.2 and 7.4, respectively), then shaken at a speed of 80 rpm and incubated at 37 °C on a water-bath thermostatic oscillator. At specific time intervals, 0.5 mL samples were withdrawn and replaced with fresh PBS to maintain a constant volume. The amount of protein in the solution was analyzed by UV/Vis Spectrophotometry at 595 nm. All investigations were performed in triplicate.

3. Results and discussion

3.1. Characterization of AAP

3.1.1. Physicochemical properties of AAP

Purified AAP was obtained by hot-water extraction, ethanol precipitation, removal of protein by the Sevag method, dialysis against distilled water and lyophilized by freeze-drying. The yield, moisture, and total sugar contents in the AAP were 4.5%, 6.2% and 90.12% (w/w), respectively. The AAP sample was water-soluble and exhibited a white flocculence. AAP did not exhibit a significant absorption peak at 280 nm by UV/Vis spectrophotometry, which indicated that the protein impurities were reduced to a very low level [23]. This result may due to the process of vacuum freeze-drying, because the water precipitated from the polysaccharide solution during freezing of the solution, changed the solution system and denatured the protein molecules finally leading to its lower solubility [24].

3.1.2. Molecular weight and SEM

Mass spectrometry was used to determine the molecular weight of AAP. The Mw of AAP ranged from 20,506.9Da to 63,923.7Da. The surface topography and structure of a polysaccharide is affected by the methods of extraction, purification and preparation used [25]. Fig. 1 shows the surface morphology of AAP dried by vacuum and lyophilization. AAP obtained by freeze-drying had continuous porous sheet shape with a loose structure, whereas the one produced by vacuum drying had a smooth surface and a spherical shape with tight structure. Comparing the two AAP products, we found that the freeze-
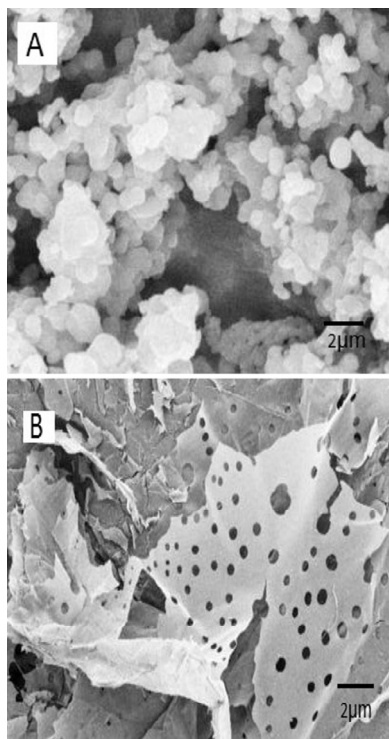

Fig. 1 – SEM images of AAP dried by (A) vacuum and (B) lyophilization.
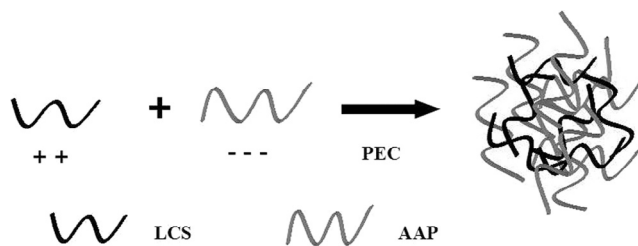

Fig. 2 – Scheme for the preparation of AAP/LCS NPs.

dried AAP dissolved more easily and faster than the other one [26].

3.2. Preparation of AAP/LCS NPs

The scheme for the preparation of AAP/LCS NPs is shown in Fig. 2. Based on the theory of polyelectrolytes [27], we investigated the feasibility of using polyelectrolyte complexes to prepare AAP/LCS NPs. When the two polysaccharide solutions were mixed by dropping, three different phenomena were observed: a clear solution, an opalescent suspension and an aggregated precipitate, where the opalescent suspension was considered to be a suspension of fine particles, in the nanometer range, that was the polyelectrolyte complexes nanoparticles. Nanoparticles could be formed using AAP with concentrations of 1.5–3.0 mg/ml and 0.5–1.5 mg/ml for LCS. Higher concentrations (>3.0 mg/ml for AAP and >1.5 mg/ml for LCS) led to aggregation, while lower concentrations (<1.5 mg/ml for AAP and <0.5 mg/ml for LCS) resulted in the formation of very few nanoparticles and, hence, the solution was clear.

The PEC process was quite gentle and involved the mixture of two aqueous phases at room temperature. The parameters, which included the effects of the pH value, AAP concentration, LCS concentration, LCS molecular weight and protein concentration on mean particle size, polydispersity index (PDI), zeta potential and entrapment efficiency of the AAP/LCS NPs were investigated, and the results are listed in Tables 1–4 and Figs. 3–7 respectively.
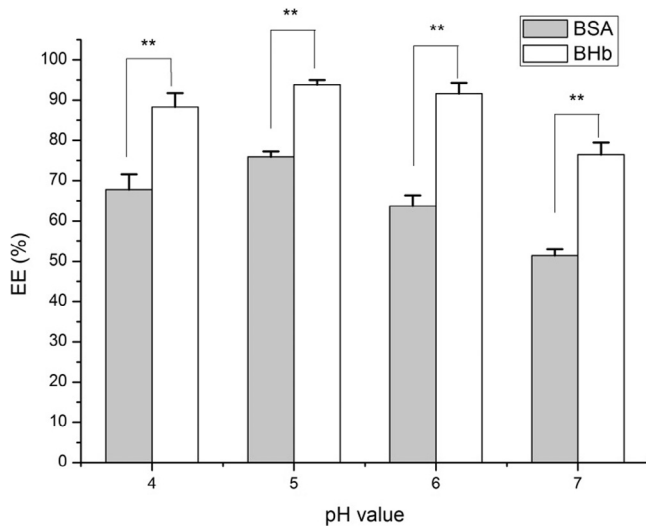
3.2.1. Effect of pH value

The effect of the pH on the particle size, and PDI of AAP/LCS NPs is shown in Table 1. When the pH ranged from 3.0 to 6.0, the AAP/LCS NPs remained relatively stable but, when the pH increased to 7.0, most of the amine groups of LCS were hardly protonated at all, leading to weaker electrostatic attractions and tangling loosely and, so the particle size of the nanoparticles

Table 1 – Effects of pH value on the particle size and PDI of AAP/LCS NPs[a].

pH value	Sizes (nm)	PDI
3.0	310.2 ± 1.7	0.175 ± 0.01
4.0	280.5 ± 3.1	0.145 ± 0.02
5.0	231.7 ± 1.9	0.189 ± 0.02
6.0	278.3 ± 2.2	0.155 ± 0.01
7.0	508.4 ± 0.6	0.181 ± 0.02

[a] LCS concentration = 1.0 mg/ml, AAP concentration = 2.5 mg/ml, LCS Mw = 25 kDa, n = 3.

Fig. 3 – Effects of pH value on the entrapment efficiency of protein-loaded AAP/LCS NPs*. *Protein concentration = 1.0 mg/ml, LCS concentration = 1.0 mg/ml, AAP concentration = 2.5 mg/ml, LCS Mw = 25 kDa, n = 3. **Indicated that P < 0.05.

was markedly increased. The AAP/LCS NPs were pH-sensitive, and this may be used for the development of drug delivery systems [28].

As shown in Fig. 3, the entrapment efficiency of BHb was higher than that of BSA at different pH values. The pI of BHb (pI = 6.8) was marginally higher than that of BSA (pI = 4.8), so, one of the reasons may be the ionic interaction between protein and AAP. BHb had a higher pI than BSA, which allowed much more positively charged BHb to be attracted and combined with negatively charged AAP. By contrast, BSA was charged negatively under the same circumstances and excluded the similarly charged AAP. Therefore, the entrapment efficiency of BHb was higher than that of BSA.

3.2.2.   *Effect of AAP concentration*
Previous studies [29,30] have indicated that the concentration of polysaccharide solution was a decisive parameter in the formation of nanoparticles by the polyelectrolyte complex method. As shown in Table 2, the particle size of AAP/LCS NPs increased from 187 to 346 nm as the concentration of AAP increased from 1.5 to 3.0 mg/ml. When the concentration of AAP was over 3.0 mg/ml, the AAP/LCS NPs tended to aggregate and

Table 2 – Effects of AAP concentration on the particle size, PDI, and zeta potential of AAP/LCS NPs[a].

AAP (mg/ml)	Sizes (nm)	PDI	Zeta potential (mV)
1.5	187.8 ± 4.8	0.144 ± 0.01	−15.9 ± 1.8
2.0	258.7 ± 3.4	0.130 ± 0.02	−17.1 ± 0.8
2.5	302.5 ± 2.9	0.092 ± 0.02	−20.5 ± 1.8
3.0	346.2 ± 5.3	0.095 ± 0.01	−27.6 ± 2.6
3.5	–	–	–

[a] LCS concentration = 1.0 mg/ml, LCS Mw = 25 kDa, n = 3.

Table 3 – Effects of LCS concentration on the particle size, PDI, and zeta potential of AAP/LCS NPs[a].

LCS (mg/ml)	Sizes (nm)	PDI	Zeta potential (mV)
0.5	186.3 ± 2.4	0.152 ± 0.02	−20.9 ± 1.5
1.0	258.6 ± 4.8	0.172 ± 0.01	−15.6 ± 2.7
1.5	526.4 ± 2.3	0.192 ± 0.02	−13.8 ± 2.2
2.0	–	–	–

[a] AAP concentration = 2.5 mg/ml, LCS Mw = 25 kDa, n = 3.

precipitate. For this reason, with the increased concentration of AAP, AAP molecules entangled with more LCS molecules so that the AAP/LCS NPs became larger and larger. The zeta potential of AAP was estimated to be −55.4 mV. This showed that the structure of AAP/LCS NPs had positive LCS chains entangled with negative AAP chains. In addition, the AAP content increase could lead to a decrease in the zeta potential of AAP/LCS NPs. In addition, the AAP content increase could lead to the decrease of the zeta potential of AAP/LCS NPs.

3.2.3.   *Effect of LCS concentration*
As shown in Table 3, the particle size increased with an increase in LCS concentration. For example, when the LCS concentration increased from 0.5 to 1.5 mg/ml, the particle size increased from 186 to 526 nm. The Zeta potential refers to the surface charge of the nanoparticles. Interestingly, the AAP/LCS NPs displayed a negative zeta potential of −20.9 mV. Compared with reported chitosan nanoparticles [31,32], the zeta potential of nanoparticles prepared with a low concentration of chitosan were negatively charged, whereas nanoparticles prepared under a high concentration of chitosan had a positive zeta potential. However, in our experiment, it was difficult to prepare positively charged AAP/LCS NPs, and this may be due to the fact that LCS chains were covered by AAP chains, which had a much higher molecular weight and a lower flexibility.

3.2.4.   *Effect of LCS Mw*
Regarding the influence of the LCS molecular weight on the particle size and PDI (in Table 4), it appeared that an increase in the LCS molecular weight might contribute to a larger particle size. When the LCS molecular weight was less than 25 kDa, very few nanoparticles were formed, and a clear solution was obtained. As the LCS molecular weight increased beyond 25 kDa, the AAP/LCS NPs particle size gradually increased. To explain this phenomena, the formation mechanism of AAP/LCS NPs needs to be discussed [33]. The formation of AAP/LCS NPs is determined by the electrostatic interaction between

Table 4 – Effects of chitosan molecular weight on the particle size, PDI of AAP/LCS NPs[a].

LCS Mw (kDa)	Sizes (nm)	PDI
10	–	–
25	213.7 ± 2.3	0.152 ± 0.02
50	261.5 ± 3.6	0.172 ± 0.03
100	329.1 ± 2.5	0.132 ± 0.02

[a] AAP concentration = 2.5 mg/ml, LCS concentration 1.0 mg/ml, n = 3.
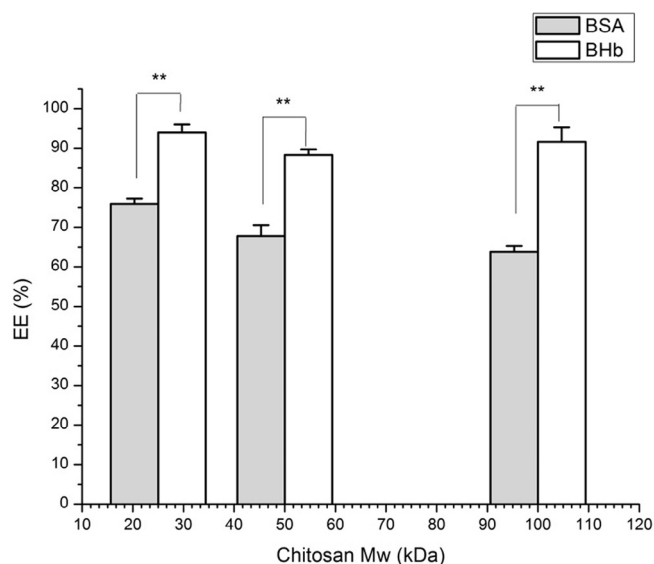
Fig. 4 – Effects of chitosan Mw on the entrapment efficiency of protein-loaded AAP/LCS NPs*. *Protein concentration = 1.0 mg/ml, LCS concentration = 1.0 mg/ml, AAP concentration = 2.5 mg/ml, $n = 3$. **Indicated that $P < 0.05$

negatively charged AAP and positively charged LCS, in this process, LCS serves as an ionic cross-linking reagent. In the cross-linking, an appropriate molecular weight of LCS is needed for the formation of nanoparticles.

As shown in Fig. 4, the molecular weight of LCS has a more marked influence on the entrapment efficiency of BSA. When the LCS molecular weight was 25 kDa, the entrapment efficiency of BSA and BHb reached a maximum, 75.9% and 93.9%, respectively. It seems that a higher molecular weight of LCS would lead to a higher encapsulation efficiency because the longer chain of LCS molecules could entrap more protein [34,35]. However, as shown in Table 4, the LCS molecular weight also affected the size of the AAP/LCS NPs. A higher molecular weight of LCS would lead to a reduction in the specific surface area of AAP/LCS NPs because of the increasing of particle size. Therefore, an appropriate LCS molecular weight is essential to obtain a high protein encapsulation efficiency.

3.2.5. Effect of protein concentration

As shown in Fig. 5, with the BSA concentration increased, the mean particle size also increased. In addition, the zeta potential increased at the same time, probably due to the loading of positively charged BSA. However, as the BHb concentration increased, the particle size also gradually increased while the zeta potential decreased rapidly for negatively charged BHb. As the protein concentration increased to 1 mg/ml (Fig. 6), the entrapment efficiency increased slightly. The high entrapment efficiency of protein could be due to the ionic interaction between AAP and protein. Too high a protein concentration may lead to aggregation [36].

3.2.6. Effect of ionic strength

The nanoparticles were fabricated by the method described, except that different amounts of NaCl were dissolved in the
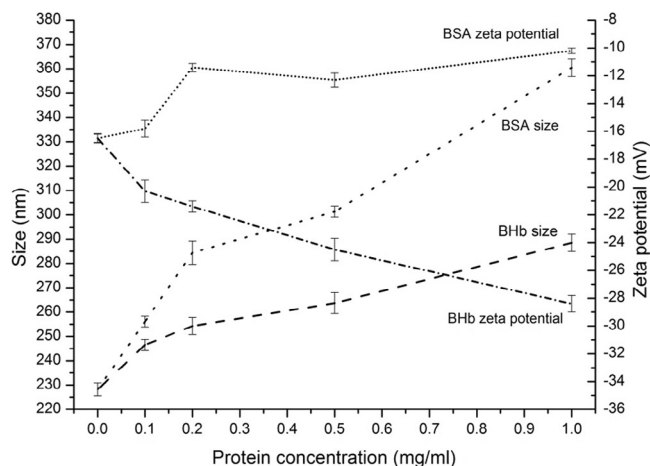
Fig. 5 – Effect of different amounts of protein (0, 0.1, 0.2, 0.5, 1.0 mg/ml) on the particle size and zeta potential*. *LCS concentration = 1.0 mg/ml, AAP concentration = 2.5 mg/ml, LCS Mw = 25 kDa, $n = 3$.

LCS solution before adding the AAP solution. The effect of ionic strength on the particle size of nanoparticles is shown in Table 5. When a low concentration of NaCl solution (0.025, 0.05 mol/L) was added, the particle size of the nanoparticles lower than those without NaCl solution while, at a high concentration of NaCl solution (0.10, 0.15 mol/l), the particle size of the nanoparticles fell sharply. This may due to the fact that the addition of NaCl favored the formation and growth of nanoparticles, as indicated in a previous study [28]. However, the addition of NaCl also weakened the electrostatic attraction between the AAP and LCS chains. Thus, at high NaCl concentrations, the effect of the interaction between the two chains exceeded the effect on the formation and growth of
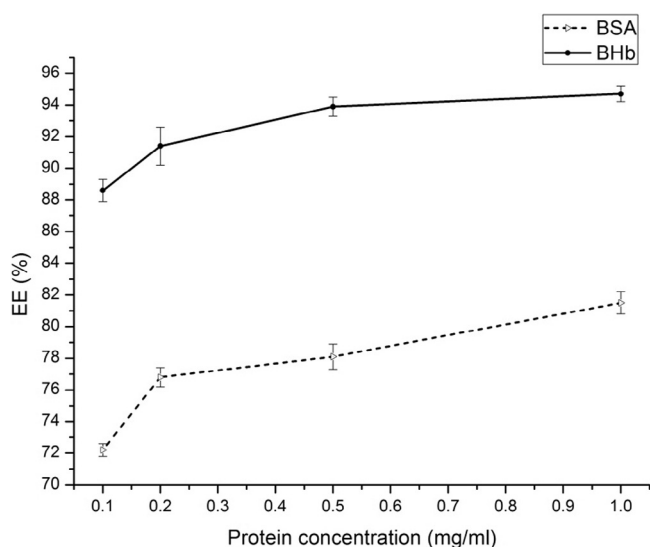
Fig. 6 – Effects of protein concentration on the entrapment efficiency of protein-loaded AAP/LCS NPs*. *LCS concentration = 1.0 mg/ml, AAP concentration = 2.5 mg/ml, LCS Mw = 25 kDa, $n = 3$.

Table 5 – Effects of NaCl concentration on the particle size, PDI of AAP/LCS NPs[a].

NaCl concentration (mol/L)	Sizes (nm)	PDI
0	245.7 ± 0.33	0.188 ± 0.02
0.025	200.5 ± 0.27	0.125 ± 0.01
0.05	224.2 ± 3.70	0.109 ± 0.02
0.10	287.3 ± 1.25	0.185 ± 0.02
0.15	328.4 ± 1.60	0.113 ± 0.02

[a] LCS concentration = 1.0 mg/ml, AAP concentration = 2.5 mg/ml, LCS Mw = 25 kDa, $n = 3$.

nanoparticles. In addition, it is very likely that AAP/LCS NPs are stable in NaCl solution.

3.3. Entrapment efficiency and loading capacity

Free protein was determined by the Coomassie blue method, and the entrapment efficiency of BSA and BHb was 81.5% and 92.6%, and the loading capacity of BSA and BHb was 32.2% and 34.1%, respectively. It is difficult to encapsulate protein completely within nanoparticles [35], owing to the electrostatic interaction between the nanoparticles and protein, most of the protein must be absorbed on the surface of the nanoparticles. Based on the results above, the entrapment efficiency could be optimized by selecting an appropriate molecular weight of LCS and optimal preparation conditions. At different pI of the protein packaged, AAP had a better loading capacity for BHb, but BSA could also have an acceptable package by adjusting the system pH. In a word, the ionic interaction between the negative charges of AAP and the state of the protein in the system plays a crucial role in effectively entrapping drugs in nanoparticles.
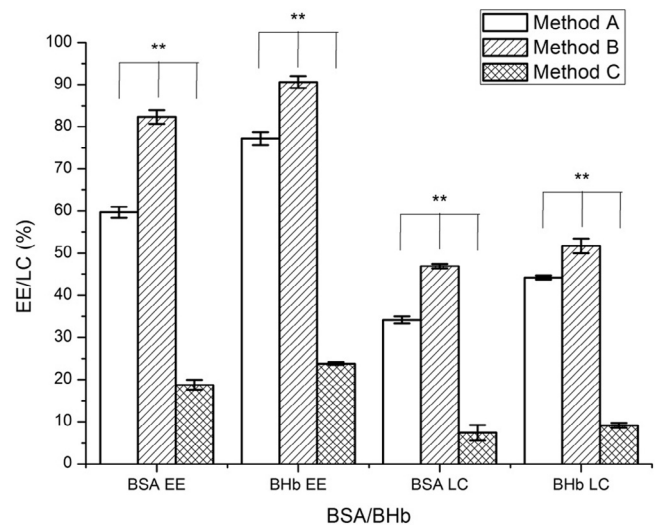
3.3.1. Effect of different preparation methods

Fig. 7 illustrated the effect of different preparation methods on entrapment efficiency and loading capacity of protein-loaded AAP/LCS NPs. In method B, protein was predissolved in the AAP solution, with a higher entrapment efficiency and loading capacity than that obtained by the other two preparation methods. This may due to ionic interaction and ionic cross-linking between positively charged BSA (pI = 4.8) and negatively charged AAP in solution (around pH 4.3) [36]. However, BHb (pI = 6.8) had a positive charge under the preparation conditions used (around pH 5) and, so, an ionic interaction would have little impact on the entrapment efficiency and loading capacity.

3.4. Characterization of AAP/LCS NPs

3.4.1. FT-IR spectra analysis

As shown in Fig. 8, for the FT-IR spectra of LCS, the characteristic peak at 1659 cm⁻¹ is attributed to protonated amino groups. The characteristic absorption peaks appearing at 1625 cm⁻¹ and 1421 cm⁻¹ can be attributed to asymmetrical and symmetrical –COO⁻ groups of AAP. These results suggest that some carboxylic groups of AAP become dissociated into –COO⁻ groups, which would be able to react with the protonated amino groups of LCS through electrostatic interactions to form poly-


Fig. 7 – Effects of different preparation methods the on entrapment efficiency and loading capacity of protein-loaded AAP/LCS NPs*. *Protein concentration = 1.0 mg/ml, LCS concentration = 1.0 mg/ml, AAP concentration = 2.5 mg/ml, LCS Mw = 25 kDa, $n = 3$. **Indicated that $P < 0.05$

electrolyte complexes [28]. Thus, the 1659 cm⁻¹ peak of –NH₂ bending vibration becomes weak and shifts to 1645 cm⁻¹ in the IR spectrum of blank nanoparticles, and the peaks of –COO⁻ in AAP shift to 1563 cm⁻¹ and 1407 cm⁻¹, respectively.

3.4.2. DSC analysis

DSC is a valid method to investigate the drug crystallinity of compounds by determining the variation in energy and temperature at the phase transition [37]. Fig. 9 shows the thermal curves of AAP, LCS and blank nanoparticles obtained by DSC. Sharp endothermic peaks of AAP and LCS were obtained at 246 °C and 230 °C, respectively, followed by decomposition which indicated the crystalline nature. The disappearance of the endothermic peak for blank nanoparticles was an indication of
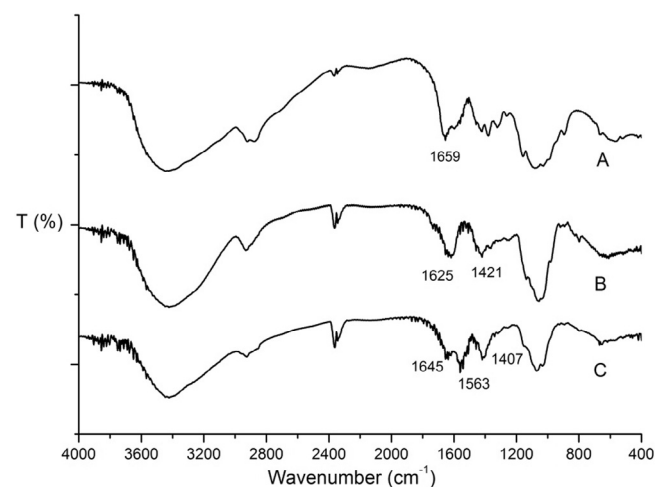
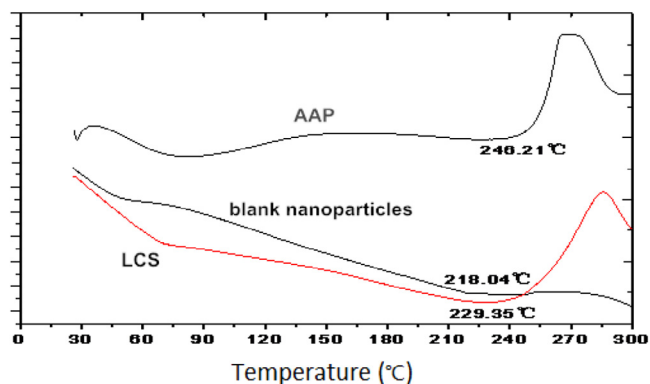**Fig. 8 – FT-IR spectra of (A) LCS, (B) AAP and (C) blank nanoparticles.**

Fig. 9 – DSC curve of AAP, LCS and blank nanoparticles.

the possible electrostatic association between the two polyions [38].

3.4.3. Particle size and TEM

The size and size distribution morphology of the AAP/LCS NPs are shown in Fig. 10 (pH 5, AAP concentration 2.5 mg/ml, LCS concentration 1.0 mg/ml, LCS Mw 25 kDa). Clearly, the nanoparticles were successfully prepared with a homogeneous size distribution and spherical morphology. The average diameter of the nanoparticles was 223 nm and PDI was 0.175.

3.5. Stability

Fig. 11 shows that the protein-loaded AAP/LCS NPs were more stable in pH 1.2 buffer than pH 7.4 buffer. At pH 7.4, because most of the carboxyl groups of AAP were in the $-COO^-$ form and the amine groups of LCS were in the $-NH_2$ form, the electrostatic attractions were weakened in the nanoparticles so that the two chains were tangled loosely and, as a result, the size of the nanoparticle increased in pH 7.4 buffer. The AAP/LCS NPs revealed a pH sensitivity, and this property may be used for the development of new drug delivery systems.

3.6. Drug release

The drug release behavior was investigated in *vitro* by dialysis in buffer solutions (pH 1.2 and pH 7.4 respectively). As shown
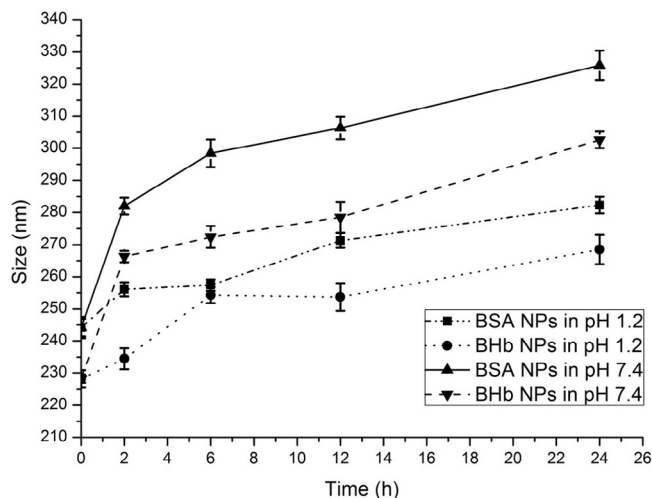

Fig. 11 – Evaluation of the size of protein-loaded AAP/LCS NPs size at different time*. *Protein concentration = 1.0 mg/ml, LCS concentration = 1.0 mg/ml, AAP concentration = 2.5 mg/ml, LCS Mw = 25 kDa, n = 3.

in Fig. 12, at pH 1.2, the amount of both BSA and BHb released from the nanoparticles was approximately 20%, which means that the AAP/LCS NPs can protect protein under acidic conditions. At pH 7.4, BSA and BHb were released from the nanoparticles in a biphasic pattern: a fast release rate in the first 5 h followed by a slow uniform release. The initial burst release of BSA from the nanoparticles indicated that part of the protein was absorbed onto the surface of nanoparticles or loosely encapsulated in nanoparticles and, then, the slow and constant release was due to the diffusion of BSA inside the nanoparticles while most of the BHb was tightly conjugated and encapsulated into the nanoparticles, and then released in a sustained fashion with decomposition of the nanoparticles. In addition, BHb was released slower than BSA because the stability of BHb NPs in pH 7.4 buffer solution was better than that of BSA NPs (as shown in Fig. 11). That means that the particle size of BSA NPs increased and allowed the BSA to be released freely from the nanoparticles. The cumulative release of BSA and BHb from AAP/LCS NPs after 24 h was 95.4% and 91.9%, respectively.
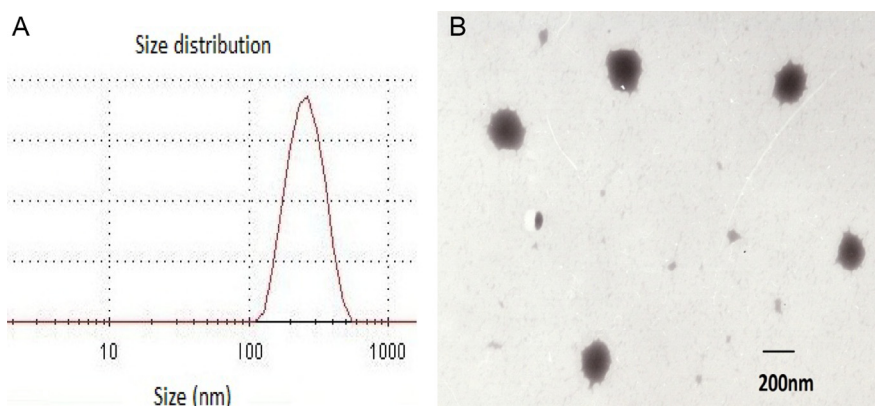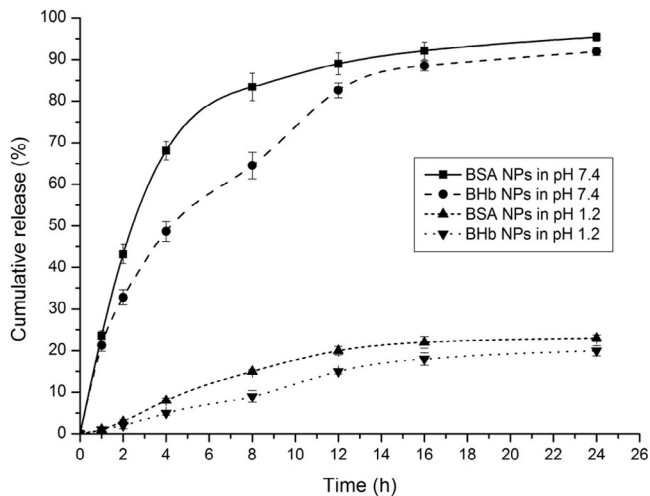

Fig. 10 – (A) Particle size distribution and (B) TEM of AAP/LCS NPs.

Fig. 12 – Cumulative release curve of BSA and BHb from nanoparticles in pH 1.2 and pH 7.4 at 37 °C.

4.   Conclusion

Regarding the novel idea for the application of AAP as a drug carrier, the results of this study demonstrated that the polysaccharide extracted and purified from auricularia auricular could be used to prepare polyelectrolyte complex nanoparticles with positively charged LCS. A small particle size and a negative zeta potential were observed. DSC and FT-IR analyses of the nanoparticles provided evidence of the formation of a polyelectrolyte complex. A higher entrapment efficiency (92.6%) was obtained for BSA-loaded AAP/LCS NPs than the BHb counterpart (82.3%). Factors such as different methods of preparation, protein concentration, pH and LCS molecular weight had a huge effect on protein loading. The in *vitro* release study showed that these protein-loaded AAP/LCS NPs were able to produce sustained release in PBS. All in all, the data reported demonstrated that AAP/LCS NPs are a promising system for the delivery of protein drugs.

Acknowledgements

REFERENCES

[1] Han C, Davis CB, Wang B, et al. Evaluation of drug candidates for preclinical development: pharmacokinetics, metabolism. Pharmacol Toxicol 2010;23:146–178.

[2] Wang T, Xu Q, Wu Y, et al. Quaternized chitosan (QCS)/poly (aspartic acid) nanoparticles as a protein drug-delivery system. Carbohydr Res 2009;344:908–914.

[3] Harush F, Rozentur E, Benita B, et al. Surface charge of nanoparticles determines their endocytic and transcytotic pathway in polarized MDCK cells. Biomacromolecules 2008;9:435–443.

[4] Sandri G, Bonferoni M, Rossi S, et al. Nanoparticles based on N-trimethylchitosan: evaluation of absorption properties using in vitro (Caco–2 cells) and ex vivo (excised rat jejunum) models. Eur J Pharm Biopharm 2007;65:68–77.

[5] Papadimitriou S, Achilias D, Bikiaris D, et al. Chitosan-g-PEG nanoparticles ionically crosslinked with poly (glutamic acid) and tripolyphosphate as protein delivery systems. Int J Pharm 2012;430:318–327.

[6] Balasse E, Odot J, Gatouillat G, et al. Enhanced immune response induced by BSA loaded in hydroxyethylstarch microparticles. Int J Pharm 2008;353:131–138.

[7] Ravi K, Bakowsky U, Lehr C, et al. Preparation and characterization of cationic PLGA nanospheres as DNA carriers. Biomaterials 2004;25:1771–1777.

[8] Salmaso S, Caliceti P. Self assembling nanocomposites for protein delivery: supramolecular interactions of soluble polymers with protein drugs. Int J Pharm 2013;440:111–123.

[9] Jadhav S, Singhal R. Pullulan-complexed alpha-amylase and glucosidase in alginate beads: enhanced entrapment and stability. Carbohydr Polym 2014;105:49–56.

[10] Li Q, Xia B, Branham M, et al. Self-assembly of carboxymethyl konjac glucomannan-g-poly(ethylene glycol) and (α-cyclodextrin) to biocompatible hollow nanospheres for glucose oxidase encapsulation. Carbohydr Polym 2011;86:120–126.

[11] Mo R, Jiang T, Di J, et al. Emerging micro- and nanotechnology based synthetic approaches for insulin delivery. Chem Soc Rev 2014;43:3595–3629.

[12] Luo Y, Wang Q. Recent development of chitosan-based polyelectrolyte complexes with natural polysaccharides for drug delivery. Int J Biol Macromol 2014;64:353–367.

[13] Liu Z, Jiao Y, Wang Y, et al. Polysaccharides-based nanoparticles as drug delivery systems. Adv Drug Deliver Rev 2008;60:1650–1662.

[14] Song Y, Zhou Y, Li Q, et al. Preparation and characterization of novel quaternized cellulose nanoparticles as protein carriers. Macromol Biosci 2009;9:857–863.

[15] Fajardo A, Lopes L, Pereira A, et al. Polyelectrolyte complexes based on pectin –NH 2 and chondroitin sulfate.et al. Carbohydr Polym 2012;87:1950–1955.

[16] Gucht J, Spruijt E, Lemmers M, et al. Polyelectrolyte complexes: bulk phases and colloidal systems. J Colloid Interface Sci 2011;361:407–422.

[17] Delair T. Colloidal polyelectrolyte complexes of chitosan and dextran sulfate towards versatile nanocarriers of bioactive molecules. Eur J Pharm Biopharm 2011;78:10–18.

[18] Wang H, Zhang H, Yuan S, et al. Molecular dynamics study of the structure of an oppositely charged polyelectrolyte and an ionic surfactant at the air/water interface. Colloids Surf A Physicochem Eng Asp 2014;454:104–112.

[19] Zeng W, Zhang Z, Gao H, et al. Characterization of antioxidant polysaccharides from Auricularia auricular using microwave-assisted extraction. Carbohydr Polym 2012;89:694–700.

[20] Zeng F, Zhao C, Pang J, et al. Chemical properties of a polysaccharide purified from solid–state fermentation of auricularia auricular and its biological activity as a hypolipidemic agent. J Food Sci 2013;78:1470–1475.

[21] Dubois M, Gilles K, Hamilton J, et al. Colorimetric method for determination of sugars and related substances. Anal Chem 1956;28:350–356.

[22] Kumar A, Ahuja M. Carboxymethyl gum kondagogu–chitosan polyelectrolyte complex nanoparticles: preparation and characterization. Int J Biol Macromol 2013;62:80–84.

[23] Hu H, Liang H, Wu Y, et al. Isolation, purification and structural characterization of polysaccharide from Acanthopanax brachypus. Carbohydr Polym 2015;127:94–100.

[24] Nam J, Park Y. Morphology of regenerated silk fibroin: effects of freezing temperature, alcohol addiction, and molecular weight. J Appl Polym Sci 2001;81:3008–3021.

[25] Elijah I, Barbara R. Characterization of grewia gum, a potential pharmaceutical excipient. J Excip Food Chem 2010;156:30–40.

[26] Kong L, Yu L, Feng T, et al. Physicochemical characterization of the polysaccharide from Bletilla striata: effect of drying method. Carbohydr Polym 2015;125:1–8.

[27] Dobrynin A, Rubinstein M. Theory of polyelectrolytes in solutions and at surfaces. Prog Polym Sci 2005;30:1049–1118.

[28] Shu S, Zhang X, Teng D, et al. Polyelectrolyte nanoparticles based on water-soluble chitosan-poly (L-aspartic acid)-polyethylene glycol for controlled protein release. Carbohydr Res 2009;344:1197–1204.

[29] Oliveira M, Ciarlini P, Feitosa J, et al. Chitosan/"angico" gum nanoparticles: synthesis and characterization. Mater Sci Eng, C 2009;29:448–451.

[30] Mihai M, Dragan E. Chitosan based nonstoichiometric polyelectrolyte complexes as specialized flocculants. Colloids Surf A Physicochem Eng Asp 2009;90:39–46.

[31] Hermans K, Van P, Everaert A, et al. Full factorial design, physicochemical characterisation and biological assessment of cyclosporine a loaded cationic nanoparticles. Eur J Pharm Biopharm 2012;82:27–35.

[32] Kim S, Fernandes M, Matamá T, et al. Chitosan–lignosulfonates sono-chemically prepared nanoparticles: characterisation and potential applications. Colloids Surf B Biointerfaces 2013;103:1–8.

[33] Naidu V, Madhusudhana K, Sashidhar R, et al. Polyelectrolyte complexes of gum kondagogu and chitosan, as diclofenac carriers. Carbohydr Polym 2009;76:464–471.

[34] Wu Y, Yang W, Wang W, et al. Chitosan nanoparticles as a novel delivery system for ammonium glycyrrhizinate. Int J Pharm 2005;295:235–245.

[35] Xu Y, Du Y. Effect of molecular structure of chitosan on protein delivery properties of chitosan nanoparticles. Int J Pharm 2003;250:215–226.

[36] Chen F, Zhang Z, Huang Y, et al. Evaluation and modification of N-trimethyl chitosan chloride nanoparticles as protein carriers. Int J Pharm 2007;336:166–173.

[37] Tian B, Luo Q, Song S, et al. Novel surface modified nanostructured lipid carriers with partially deacetylated water soluble chitosan for efficient ocular delivery. J Pharm Sci 2012;101:1040–1049.

[38] Silva M, Cocenza D, Grillo R, et al. Paraquat-loaded alginate/chitosan nanoparticles: preparation, characterization and soil sorption studies. J Hazard Mater 2011;190:366–374.